

Isotropization and Hydrodynamization in Weakly Coupled Heavy-Ion Collisions

Aleksi Kurkela^{1,2} and Yan Zhu³

¹*Physics Department, Theory Unit, CERN, CH-1211 Genève 23, Switzerland*

²*Faculty of Science and Technology, University of Stavanger, 4036 Stavanger, Norway*

³*Departamento de Física de Partículas and IGFAE, Universidade de Santiago de Compostela, E-15706 Santiago de Compostela, Galicia, Spain*

(Received 14 July 2015; published 27 October 2015)

We numerically solve the $(2+1)$ -dimensional effective kinetic theory of weak coupling QCD under longitudinal expansion, relevant for early stages of heavy-ion collisions. We find agreement with viscous hydrodynamics and classical Yang-Mills simulations in the regimes where they are applicable. By choosing initial conditions that are motivated by a color-glass-condensate framework, we find that for $Q_s = 2$ GeV and $\alpha_s = 0.3$ the system is approximately described by viscous hydrodynamics well before $\tau \lesssim 1.0$ fm/c.

DOI: 10.1103/PhysRevLett.115.182301

PACS numbers: 12.38.Mh, 05.70.Ln

Introduction.—In the weak-coupling picture of the pre-thermal evolution of heavy-ion collisions, the postcollision debris that ends up in the midrapidity region undergoes several stages that are characterized by widely different physics and degrees of freedom. On the one hand, according to the saturation paradigm [1], at very early times $\tau \sim Q_s^{-1}$, where Q_s is the typical energy scale right after the collision, the energy is deposited in strong color fields. These strong fields admit a description in terms of classical Yang-Mills theory to leading order in the 't Hooft coupling $\lambda = 4\pi N_c \alpha_s$. Indeed, there have been several interesting studies of classical Yang-Mills fields under longitudinal expansion in recent years [2–6]. On the other hand, once the system has reached a local thermal equilibrium, or at least is approximately isotropized [7], the matter in the midrapidity region (at sufficiently low p_T) is described by relativistic fluid dynamics [8,9]. There has been a sizable and very successful program of numerical simulations of relativistic hydrodynamics.

It is well known that classical Yang-Mills theory cannot reach thermalization due to the Rayleigh-Jeans catastrophe, and neither can it isotropize when exposed to rapid longitudinal expansion, as noticed by [10]. Instead, classical evolution drives the system further away from equilibrium, making the system less occupied (i.e., having weaker fields) but more anisotropic, which has also been observed in the simulations of [4,5]. Therefore, there is a missing link between the physics of saturated gluon fields and fluid dynamics that needs to be bridged in order to fully carry the predictions of saturation physics to the hydrodynamic regime. This gap can be filled with the systematically improvable framework of effective kinetic theory (EKT), from Ref. [11].

EKT faithfully describes, to leading order in λf systems, where the typical occupancies of gluons are not nonperturbative, $f \ll 1/\lambda$, and where they have momentum significantly larger than the in-medium screening scale $p^2 > m^2 \equiv \lambda \int_{\mathbf{p}} f(p)/p$. At weak coupling, these conditions are certainly fulfilled in thermal equilibrium and, therefore, we can describe the system all the way to the equilibrium. While these conditions are not fulfilled at the very earliest times, both EKT and classical Yang-Mills theory give an equally valid leading-order description for a wide range of large but perturbative occupancies, $1 \ll f \ll 1/\lambda$ [12,13]. Therefore, a possible strategy to simulate the system through all time scales is to start the simulation with a classical Yang-Mills simulation (for $Q_s \tau \sim 1$ and $f \sim 1/\lambda$) and, subsequently, pass the system to EKT at some arbitrary time $\tau_{\text{EKT}} Q_s \gg 1$. Then, once EKT has brought the system sufficiently close to the thermal equilibrium, both hydrodynamics and EKT should give equivalent descriptions, and the system can be passed to a hydrodynamical simulation at some arbitrary time τ_{hydro} .

The proof of principle of such a procedure was shown in a series of papers [13–15] in an isotropic setting in the absence of expansion. Here, we present the first results of numerical simulations of the EKT in a boost-invariant $(2+1)$ D setting and demonstrate the connection with both classical Yang-Mills simulations and viscous hydrodynamics. We make a first attempt to model the early stages of heavy-ion collision starting from the overoccupied region all the way to the thermal equilibrium, and we find that after time $Q_s \tau \sim 5.0$ the time evolution of energy density is described by viscous hydrodynamics to a better-than-10% accuracy for a realistic coupling $\lambda = 10$ corresponding to $\alpha_s \approx 0.3$.

The current result, however, is incomplete in two ways. First, there have been significant steps to describe the melting of the strong color fields in classical statistical field theory [2,3,6], but currently we do not have a reliable initial state from a $(3+1)$ D simulation to enter into our EKT simulation. Therefore we initialize our system at $Q_s \tau \sim 1$ with

Published by the American Physical Society under the terms of the Creative Commons Attribution 3.0 License. Further distribution of this work must maintain attribution to the author(s) and the published article's title, journal citation, and DOI.

the energy density given by a (2 + 1)D simulation [16], and we vary the parameters of the initial condition to quantify the ignorance of the very-early-time dynamics. Second, certain nonperturbative chromo-Weibel instabilities [17] arising from anisotropic screening play a parametrically leading-order role during the whole nonequilibrium evolution [18,19]. However, numerical simulations of classical fields [6] have not been able to see these instabilities beyond the very early times. This suggests that even though the instabilities contribute formally at leading order, their effect is numerically small for values of λ that are phenomenologically interesting. Therefore, because a formally correct treatment of anisotropic screening is rather complicated [20–23] and not a fully solved problem, we in this Letter will treat the screening in an isotropic way. Therefore, our results are correct to leading order in λ for systems that are close to isotropy (late times), and for large anisotropies our results have leading logarithmic accuracy apart from the instabilities.

Methodology.—The EKT of [11] is defined though the effective Boltzmann equation for the color- and spin-averaged distribution function of gluons, and to leading order in λ , it contains effective $2 \leftrightarrow 2$ scattering and $1 \leftrightarrow 2$ splitting terms,

$$-\frac{df_{\mathbf{p}}}{d\tau} = C_{1 \leftrightarrow 2}[f_{\mathbf{p}}] + C_{2 \leftrightarrow 2}[f_{\mathbf{p}}] + C_{\text{exp}}[f_{\mathbf{p}}]. \quad (1)$$

We restrict ourselves to azimuthally symmetric distributions but allow anisotropy in the \mathbf{z} direction, so that it is enough to specify $f_{\mathbf{p}} = f_{x_p, p}$ with $x_p \equiv \hat{\mathbf{z}} \cdot \hat{\mathbf{p}}$. The effect of longitudinal expansion is encapsulated in $C_{\text{exp}}[f](\mathbf{p}) = -(p_z/\tau)(\partial/\partial p_z)f(\mathbf{p})$ [24].

The $2 \leftrightarrow 2$ effective scattering term reads

$$\begin{aligned} C_{2 \leftrightarrow 2}[f](\tilde{\mathbf{p}}) &= \frac{(2\pi)^3}{4\pi\tilde{p}^2} \frac{1}{8\nu} \int d\Gamma_{\text{PS}} |\mathcal{M}|^2 (f_{\mathbf{p}} f_{\mathbf{k}} g_{\mathbf{p}'} g_{\mathbf{k}'} - f_{\mathbf{p}'} f_{\mathbf{k}'} g_{\mathbf{p}} g_{\mathbf{k}}) \\ &\times [\delta(\tilde{\mathbf{p}} - \mathbf{p}) + \delta(\tilde{\mathbf{p}} - \mathbf{k}) - \delta(\tilde{\mathbf{p}} - \mathbf{p}') - \delta(\tilde{\mathbf{p}} - \mathbf{k}')], \end{aligned} \quad (2)$$

where $\nu = 2d_A$ and $g_{\mathbf{p}} \equiv 1 + f_{\mathbf{p}}$. $d\Gamma_{\text{PS}}$ is the integral measure over the phase space of $2 \leftrightarrow 2$ processes, singling out the z direction

$$\begin{aligned} \int d\Gamma_{\text{PS}} &\equiv \frac{1}{2^{11}\pi^7} \int_0^\infty dq \int_{-q}^q d\omega \int_{(q-\omega)/2}^\infty dp \int_{(q+\omega)/2}^\infty dk \\ &\times \int_{-1}^1 dx_q \int_0^{2\pi} d\phi_{pq} d\phi_{kq}. \end{aligned} \quad (3)$$

In these coordinates the angles of incoming and outgoing momenta read

$$x_{\{p\}} = -\sin\theta_{\{p\}q} \cos\phi_{\{p\}q} \sqrt{1 - x_q^2} + \cos\theta_{\{p\}q} x_q. \quad (4)$$

This relation holds for x_k , $x_{p'}$, and $x_{k'}$ with $\cos\phi_{p'q} = \cos\phi_{pq}$, $\cos\phi_{k'q} = \cos\phi_{kq}$,

$$\cos\theta_{pq} = \frac{\omega}{q} + \frac{t}{2pq}, \quad \cos\theta_{kq} = \frac{\omega}{q} - \frac{t}{2kq}, \quad (5)$$

$$\cos\theta_{p'q} = \frac{\omega}{q} - \frac{t}{2p'q}, \quad \cos\theta_{k'q} = \frac{\omega}{q} + \frac{t}{2k'q}, \quad (6)$$

and $t \equiv \omega^2 - q^2$. The effective matrix element for most kinematics is the ordinary vacuum tree-level element

$$\frac{|\mathcal{M}|^2}{16\lambda^2 d_A} = \left(\frac{9}{4} + \frac{(s-t)^2}{u^2} + \frac{(u-s)^2}{t^2} + \frac{(t-u)^2}{s^2} \right). \quad (7)$$

For small $t \sim m^2$ or $u \sim m^2$ the tree-level element has an IR divergence that is regulated by the physics of screening. In the formulation of [11], the screening is treated by replacing the naive tree-level matrix element by the retarded hard-thermal-loop resummed expression in the soft kinematic region. The resummed propagator in the anisotropic case, however, contains a nonintegrable singularity, signaling the presence of an instability in the system. Therefore, this procedure is not fully satisfactory in the anisotropic system. In this Letter we will restrict ourselves to isotropic screening and we use the prescription derived in [13], replacing

$$q^2 t \rightarrow t(q^2 + 2\xi_0^2 m^2) \quad (8)$$

in the denominator with $\xi_0 = e^{5/6}/\sqrt{8}$ (and using a similar process for u), which is accurate to leading order in the case of isotropic distribution.

The effective $1 \leftrightarrow 2$ collinear splitting term reads

$$\begin{aligned} C_{1 \leftrightarrow 2}[f](\tilde{\mathbf{p}}) &= \frac{(2\pi)^3}{4\pi\tilde{p}^2} \frac{1}{\nu} \int_0^\infty dp \int_0^{p/2} dk' [4\pi\gamma(p; p', k')] \\ &\times (f_{x_p, p} g_{x_p, p'} g_{x_p, k'} - g_{x_p, p} f_{x_p, p'} f_{x_p, k'}) \\ &\times [\delta(\tilde{p} - p) - \delta(\tilde{p} - p') - \delta(\tilde{p} - k')], \end{aligned} \quad (9)$$

where $p' = p - k'$, and the effective splitting rate reads

$$\gamma(p; p', k') = \frac{p^4 + p'^4 + k'^4}{p^3 p'^3 k'^3} \frac{d_A \lambda}{2(2\pi)^3} \int \frac{d^2 h}{(2\pi)^2} 2\mathbf{h} \cdot \text{Re}\mathbf{F}.$$

Again, consistently assuming only isotropic screening, the function \mathbf{F} is given by the solution to the linear integral equation

$$\begin{aligned} 2\mathbf{h} &= i\delta E(\mathbf{h})\mathbf{F}(\mathbf{h}) + \frac{\lambda T_*}{2} \int \frac{d^2 q}{(2\pi)^2} [\mathcal{A}(\mathbf{q}) \\ &\times (3\mathbf{F}(\mathbf{h}) - \mathbf{F}(\mathbf{h} - p\mathbf{q}) - \mathbf{F}(\mathbf{h} - k\mathbf{q}) - \mathbf{F}(\mathbf{h} + p'\mathbf{q}))]. \end{aligned} \quad (10)$$

$T_* = (\lambda/2m^2) \int (d^3 p)/[(2\pi)^3] f_{\mathbf{p}}(1 + f_{\mathbf{p}})$, and $\delta E = m^2/p' + m^2/k' - m^2/p + \mathbf{h}^2/2pk'p'$. We solve this equation using an efficient numerical method introduced in [25].

For the numerical solution of the EKT, we discretize $n_{x_p, p} = 4\pi p^2/(2\pi)^3 f_{x_p, p}$ on a 2D grid and Monte Carlo estimate the integrals of Eqs. (3),(9). We use a

logarithmically spaced grid for both p and x_p , with at least 250 grid points in the angular direction and at least 100 in the p direction. We vary the number of grid points to verify that the results are insensitive to the number of grid points. Our algorithm, the discrete- p method of [13], conserves energy exactly and has exactly correct particle number violation for the $1 \leftrightarrow 2$ term.

Results.—We shall now apply EKT to simulate the prethermal evolution of the expanding fireball created in a heavy-ion collision. In a saturation framework, the initial condition is typically described in terms of “gluon liberation coefficient” c and mean transverse momentum $\langle p_T \rangle / Q_s$ [26,27]. The gluon liberation coefficient is proportional to the total gluon multiplicity per unit rapidity,

$$2d_A\tau \int \frac{d^3p}{(2\pi)^3} f \equiv \frac{dN_{\text{init,g}}}{d^2\mathbf{x}_\perp dy} = c \frac{d_A Q_s^2}{\pi\lambda}, \quad (11)$$

after the classical fields have decohered, and it can be described in terms of quasiparticles. Lappi [16] finds, in a JIMWLK-evolved McLerran-Venugopalan model, values relevant for heavy-ion collisions and for the LHC that are of roughly $\langle p_T \rangle \approx 1.8Q_s$ and $c \approx 1.25$, extracted at time $Q_s\tau = 12$ from a 2D classical Yang-Mills simulation. By construction, the distribution then has $\langle p_z \rangle = 0$. It has, however, been noted [28] that certain plasma instabilities will broaden the distribution in p_z in a time scale $Q\tau \sim 1/\log^2(\lambda^{-1})$. Therefore, as a rough estimate of the initial condition, we instead take, somewhat arbitrarily, our initial condition at the time $Q\tau = 1$ to be

$$f(p_z, p_\perp) = \frac{2}{\lambda} A f_0(p_z \xi / \langle p_T \rangle, p_\perp / \langle p_T \rangle), \quad (12)$$

$$f_0(\hat{p}_z, \hat{p}_\perp) = \frac{1}{\sqrt{\hat{p}_\perp^2 + \hat{p}_z^2}} e^{-2(\hat{p}_\perp^2 + \hat{p}_z^2)/3}, \quad (13)$$

choosing A such that comoving energy density $\tau\epsilon = \langle p_T \rangle dN/d^2\mathbf{x}_\perp dy$ is fixed. We then vary $\xi = 4, 10$ to quantify our ignorance of the initial nonperturbative dynamics.

Figure 1 displays a set of trajectories from simulations with varying λ and $\xi = 4, 10$ on a plane of mean occupancy (weighted by the energy of particles) and anisotropy measured by the ratio of the transverse and longitudinal pressures P_T/P_L . The line with $\lambda = 0$ corresponds to the classical field limit $\lambda \rightarrow 0$ with fixed λf , which is obtained in EKT by including only the highest power of f 's in Eqs. (2),(9). The classical field theory cannot thermalize and, indeed, it flows instead to a stationary scaling solution. By performing classical Yang-Mills simulations, Berges *et al.* have established that the scaling solution can be described by a scaling form of the distribution function [4],

$$f(p_z, p_\perp, \tau) = (Q_s\tau)^{-2/3} f_S((Q_s\tau)^{1/3} p_z, p_\perp), \quad (14)$$

where f_S is approximately constant as a function of time. This behavior is demonstrated in Fig. 2, where we plot a section of rescaled distribution function f_S measured at various times as a function for $\tilde{p}_z \equiv (Q_s\tau)^{1/3} p_z$ at fixed p_\perp

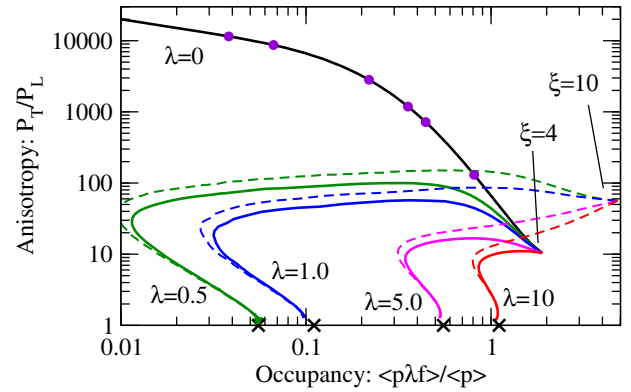


FIG. 1 (color online). Trajectories of runs with different initial conditions $\xi = 4$ (Solid lines) and $\xi = 10$ (dashed lines) and varying coupling λ in a plane of mean occupancy (weighted by the energy of particles) and anisotropy. The $\lambda = 0$ line corresponds to the classical field approximation. The violet dots refer to the times in Fig. 2. The simulations at finite coupling reach thermal equilibrium located at the points indicated by the black crosses.

following Berges *et al.* Our results corroborate that such a scaling solution exists at late times within the classical approximation, and we observe that the scaling regime is reached after a time $Q_s\tau \sim 15$.

Moving on to the finite but small coupling $\lambda = 1, 0.5$, we see qualitative agreement with the parametric picture of bottom-up thermalization from Ref. [10]. Three distinct stages of evolution are visible. In the first stage, the classical evolution drives the system to be more anisotropic and less occupied. Once the occupancies reach $f \sim 1$, there is a qualitative change in the dynamics of the system, as Bose enhancement is lost. This has the effect that anisotropy remains steady, but the system continues to become more dilute. Only in the last stage, which is characterized by a radiational breakup of the particles at the scale Q_s , does the trajectory turn back and reach thermal equilibrium, denoted by the black crosses in Fig. 1. For larger values of coupling $\lambda = 5.0, 10$, however, these features become less pronounced, and the system

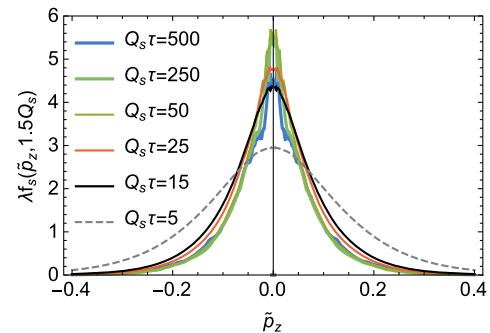


FIG. 2 (color online). Sections of scaled distribution $f_S(\tilde{p}_z, p_\perp) = (Q_s\tau)^{2/3} f[\tilde{p}_z(Q_s\tau)^{-1/3}, p_\perp]$ at $p_\perp = 1.5Q_s$ in the classical approximation at vastly different times. The good overlap of the curves indicates that system has reached the classical scaling solution of Eq. (14). In contrast, $Q_s\tau = 5$ has not yet reached the scaling solution.

takes a more straight trajectory towards equilibrium. It should be noted that for these values of λ the assumption of $p \gg m$ is not satisfied and large next-to-leading-order corrections are to be expected.

Approach to hydrodynamics.—We expect that late-time evolution should be described by relativistic hydrodynamics. Under flow with translational invariance along transverse directions and boost invariance, the hydrodynamical relations read, to second order in gradients [29],

$$\partial_\tau \epsilon = -\frac{4\epsilon}{3\tau} + \frac{\Phi}{\tau}, \quad (15)$$

$$\partial_\tau \Phi = -\frac{\Phi}{\tau_\Pi} + \frac{4\eta}{3\tau_\Pi\tau} - \frac{4}{3\tau}\Phi - \frac{\lambda_1}{2\tau_\Pi\eta^2}\Phi^2, \quad (16)$$

with longitudinal and transverse pressure $P_L = \frac{1}{3}\epsilon - \Phi$ and $P_T = \frac{1}{3}\epsilon + \frac{1}{2}\Phi$. The first-order hydrodynamics corresponds to setting $\Phi = 4\eta/3\tau$ in Eq. (15). At weak coupling, the transport coefficients η , τ_Π , and λ_1 are known [30,31], leaving zero free parameters to fit, aside from the time when the hydrodynamics is initialized. We initialize the first-order hydrodynamics at the latest time we have in our simulation and integrate Eq. (15) backwards in time. For the second-order hydrodynamics, integrating backwards is highly unstable; we initialize the energy density at some arbitrary earlier time and integrate forwards in time.

In Fig. 3 we examine the validity of the hydrodynamical expansion at small $\lambda = 1$ and at realistic intermediate $\lambda = 10$ ($\alpha_s \approx 0.3$) values of coupling. In both cases we see that the evolution of the components of the energy-momentum tensor asymptotes to their hydrodynamical values. In case of $\lambda = 1$, the hydrodynamical behavior is reached only at a rather late time, $Q_s\tau \sim 2000$. We have checked that including second-order terms before this time does not make the convergence significantly better; before this time, the evolution differs qualitatively from the hydrodynamical prediction. However, rather remarkably, for $\lambda = 10$ even first-order hydrodynamics gives a very good description of the data all the way to very early times, $Q_s\tau \sim 10$ (corresponding to $\tau \sim 1$ fm/c for $Q_s = 2.0$ GeV) where the ratio of the pressures is still as large as $P_T/P_L \approx 5$. In addition, including the second-order terms significantly improves the convergence. Indeed, we find that initializing the second-order hydrodynamics at $Q_s\tau = 1$ leads to only 10% relative error in the energy density at late times.

Discussion and conclusion.—The parametric estimate of Baier *et al.* [10] for the time when the hydrodynamic behavior sets in is $Q_s\tau \sim \lambda^{-13/5}$. This arises from equating the age of the system (τ) with the time scale (τ_Q) it takes to affect appreciably the scale Q_s in a thermal bath whose temperature depends on this time $T(\tau) \sim \lambda^{-1/4}Q_s(Q_s\tau)^{-1/4}$, according to conservation of comoving energy density. In [10] it was assumed that the rate for affecting the scale Q_s is Landau-Pomeranchuk-Migdal suppressed [32], giving $\tau_Q \sim (Q_s/T)^{1/2}/\lambda^2 T$. A self-consistent solution of these equations gives the aforementioned estimate of [10]. Arnold

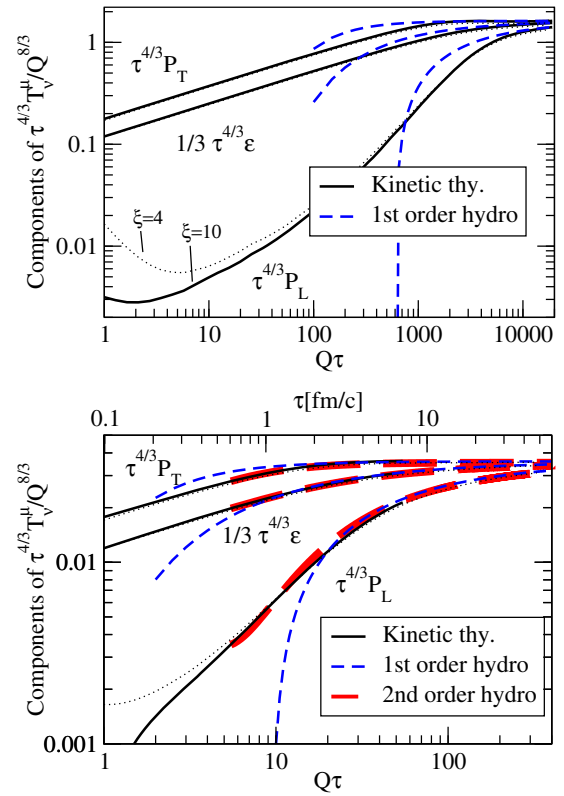


FIG. 3 (color online). Longitudinal pressure P_L , energy density ϵ , and transverse pressure P_T from a simulation with $\xi = 10.0$ and $\lambda = 1$ (top panel) and $\lambda = 10$ (bottom panel). The components of T^μ_ν have been scaled by $\tau^{4/3}$ so that the ideal hydrodynamics corresponds to horizontal lines. The scale on the x axis with fm/c corresponds to $Q_s = 2.0$ GeV ≈ 10 /fm. The simulations with $\xi = 4$ are also displayed with thin dotted lines.

and Lenaghan [33] noted that as the scattering rate in thermal plasma is $\tau_Q \sim 1/\lambda^2 T$, there can be no process that would make the estimate faster than $Q_s\tau \sim \lambda^{-7/3}$. We have examined the validity of these scaling estimates by plotting the difference of the energy density obtained from the simulation and the first-order hydrodynamic estimate, and we find that both of these estimates describe the data poorly. However, if we assume that the approach is governed by the hydrodynamical relaxation time $\tau_Q \sim \tau_\Pi \sim \eta/sT$, we get an estimate $\tau \sim \lambda^{1/3}(\eta/s)^{4/3}/Q_s$. Figure 4 displays the deviation of the hydrodynamics as a function of rescaled time. In particular, for intermediate couplings $\lambda = 5, 10$, the overlap of the different curves indicates correct scaling. Note that this estimate is parametrically the same as the estimate of Arnold and Lenaghan because, parametrically, $\eta/s \sim \lambda^{-2}$. However, there are large corrections beyond the parametric estimate in η/s ; because of these, it is important to use the full numerical result instead of the simpler parametric estimate. We believe, though, in the absence of plasma instabilities, that the correct scaling at sufficiently small λ is that of [10]. This estimate is, however, based on a large-scale separation of $T(\tau_{\text{hydro}})/Q_s \sim \lambda^{2/5}$. Numerically this ratio is not very large,

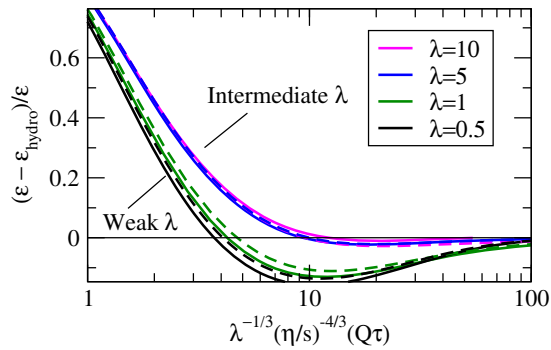


FIG. 4 (color online). Scaling of the approach to first-order hydrodynamics at various values of λ . The dashed lines correspond to $\xi = 4$ and the solid ones to $\xi = 10$.

even in our simulation with small $\lambda = 1.0$ where the ratio is $T/Q_s \approx 0.15$ (at $Q_s \tau = 1800$), as can be inferred from Fig. 3. Therefore, we believe that the scaling predicted by [10] sets in only at significantly smaller couplings.

In conclusion, we have shown how a far-from-equilibrium overoccupied configuration of gluons reaches hydrodynamical flow under longitudinal expansion in a weak-coupling setting that is systematically improvable. It has been demonstrated by Chesler and Yaffe within an AdS/CFT framework that at large values of 't Hooft coupling, hydrodynamics is surprisingly robust, even in the presence of large anisotropy [34]. The main deliverable of this Letter is to show that this robustness is present also in the weak-coupling picture extrapolated to intermediate couplings relevant for heavy-ion collisions.

The authors thank Stefan Floerchinger, Liam Keegan, Tuomas Lappi, Guilherme Milhano, Guy Moore, and Urs Wiedemann for useful discussions. Y. Z. is supported by the European Research Council, Grant No. HotLHC ERC-2011-StG-279579.

[1] E. Iancu, A. Leonidov, and L. McLerran, [arXiv:hep-ph/0202270](#); E. Iancu and R. Venugopalan, in *Quark-Gluon Plasma 3*, edited by R. C. Hwa *et al.* (World Scientific, Singapore, 2004); F. Gelis, T. Lappi, and R. Venugopalan, *Int. J. Mod. Phys. E* **16**, 2595 (2007); F. Gelis, E. Iancu, J. Jalilian-Marian, and R. Venugopalan, *Annu. Rev. Nucl. Part. Sci.* **60**, 463 (2010).

[2] T. Epelbaum and F. Gelis, *Phys. Rev. Lett.* **111**, 232301 (2013).

[3] T. Epelbaum and F. Gelis, *Phys. Rev. D* **88**, 085015 (2013).

[4] J. Berges, K. Boguslavski, S. Schlichting, and R. Venugopalan, *Phys. Rev. D* **89**, 114007 (2014).

[5] J. Berges, K. Boguslavski, S. Schlichting, and R. Venugopalan, *Phys. Rev. D* **89**, 074011 (2014).

[6] J. Berges, B. Schenke, S. Schlichting, and R. Venugopalan, *Nucl. Phys. A* **931**, 348 (2014).

[7] P. B. Arnold, J. Lenaghan, G. D. Moore, and L. G. Yaffe, *Phys. Rev. Lett.* **94**, 072302 (2005).

[8] D. Teaney, J. Lauret, and E. V. Shuryak, *Phys. Rev. Lett.* **86**, 4783 (2001); P. Huovinen, P. F. Kolb, U. W. Heinz, P. V. Ruuskanen, and S. A. Voloshin, *Phys. Lett. B* **503**, 58 (2001); P. F. Kolb, U. W. Heinz, P. Huovinen, K. J. Eskola,

and K. Tuominen, *Nucl. Phys. A* **696**, 197 (2001); T. Hirano and K. Tsuda, *Phys. Rev. C* **66**, 054905 (2002); P. F. Kolb and R. Rapp, *Phys. Rev. C* **67**, 044903 (2003).

[9] R. Baier, P. Romatschke, and U. A. Wiedemann, *Phys. Rev. C* **73**, 064903 (2006); P. Romatschke and U. Romatschke, *Phys. Rev. Lett.* **99**, 172301 (2007); M. Luzum and P. Romatschke, *Phys. Rev. C* **78**, 034915 (2008); **79**, 039903(E) (2009); K. Dusling and D. Teaney, *Phys. Rev. C* **77**, 034905 (2008); H. Song and U. W. Heinz, *Phys. Rev. C* **77**, 064901 (2008).

[10] R. Baier, A. H. Mueller, D. Schiff, and D. T. Son, *Phys. Lett. B* **502**, 51 (2001).

[11] P. B. Arnold, G. D. Moore, and L. G. Yaffe, *J. High Energy Phys.* **01** (2003) 030.

[12] A. H. Mueller and D. T. Son, *Phys. Lett. B* **582**, 279 (2004); V. Mathieu, A. H. Mueller, and D. N. Triantafyllopoulos, *Eur. Phys. J. C* **74**, 2873 (2014).

[13] M. C. Abreu, A. Kurkela, E. Lu, and G. D. Moore, *Phys. Rev. D* **89**, 074036 (2014).

[14] A. Kurkela and G. D. Moore, *Phys. Rev. D* **86**, 056008 (2012).

[15] A. Kurkela and E. Lu, *Phys. Rev. Lett.* **113**, 182301 (2014).

[16] T. Lappi, *Phys. Lett. B* **703**, 325 (2011).

[17] S. Mrowczynski, *Phys. Lett. B* **214**, 587 (1988); **656**, 273 (2007); **314**, 118 (1993); S. Mrowczynski and M. H. Thoma, *Phys. Rev. D* **62**, 036011 (2000).

[18] A. Kurkela and G. D. Moore, *J. High Energy Phys.* **11** (2011) 120.

[19] A. Kurkela and G. D. Moore, *J. High Energy Phys.* **12** (2011) 044.

[20] P. Romatschke, *Phys. Rev. C* **75**, 014901 (2007).

[21] P. Romatschke and M. Strickland, *Phys. Rev. D* **68**, 036004 (2003); P. Romatschke and M. Strickland, *Phys. Rev. D* **70**, 116006 (2004).

[22] P. B. Arnold, G. D. Moore, and L. G. Yaffe, *Phys. Rev. D* **72**, 054003 (2005).

[23] D. Bodeker and K. Rummukainen, *J. High Energy Phys.* **07** (2007) 022.

[24] A. H. Mueller, *Phys. Lett. B* **475**, 220 (2000).

[25] J. Ghiglieri and G. D. Moore, *J. High Energy Phys.* **12** (2014) 029.

[26] A. H. Mueller, *Nucl. Phys. B* **572**, 227 (2000).

[27] Y. V. Kovchegov, *Nucl. Phys. A* **692**, 557 (2001).

[28] P. Romatschke and R. Venugopalan, *Phys. Rev. Lett.* **96**, 062302 (2006); P. Romatschke and R. Venugopalan, *Eur. Phys. J. A* **29**, 71 (2006); P. Romatschke and R. Venugopalan, *Phys. Rev. D* **74**, 045011 (2006); H. Iida, T. Kunihito, B. Müller, A. Ohnishi, A. Schaefer, and T. T. Takahashi, *Phys. Rev. D* **88**, 094006 (2013).

[29] R. Baier, P. Romatschke, D. T. Son, A. O. Starinets, and M. A. Stephanov, *J. High Energy Phys.* **04** (2008) 100.

[30] P. B. Arnold, G. D. Moore, and L. G. Yaffe, *J. High Energy Phys.* **05** (2003) 051.

[31] M. A. York and G. D. Moore, *Phys. Rev. D* **79**, 054011 (2009).

[32] L. D. Landau and I. Pomeranchuk, *Dokl. Akad. Nauk Ser. Fiz.* **92**, 535 (1953); A. B. Migdal, *Phys. Rev.* **103**, 1811 (1956); R. Baier, Y. L. Dokshitzer, A. H. Mueller, S. Peigne, and D. Schiff, *Nucl. Phys. B* **484**, 265 (1997).

[33] P. B. Arnold and J. Lenaghan, *Phys. Rev. D* **70**, 114007 (2004).

[34] P. M. Chesler and L. G. Yaffe, *Phys. Rev. D* **82**, 026006 (2010); P. M. Chesler and L. G. Yaffe, *Phys. Rev. Lett.* **106**, 021601 (2011); P. M. Chesler and L. G. Yaffe, [arXiv:1501.04644](#).